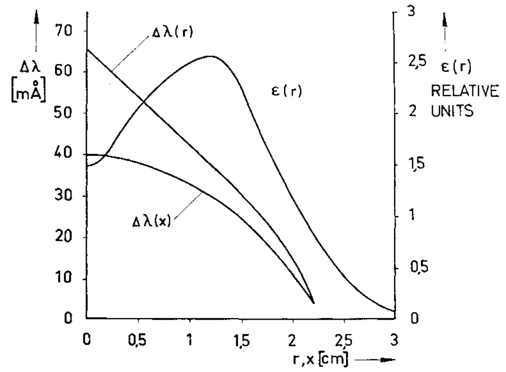

Fig. 3 Measured and transformed Doppler shifts.

the axial velocity of the plasma jet were measured at Secs. IV and V (Fig. 2) in a manner similar to the one mentioned previously. The two interferograms, however, were taken upstream and downstream, respectively, at an angle of 60° against the axis of the plasma jet, thus experimentally eliminating the rotational parts of the line shifts as a first-order approximation. Profiles of relative intensities which were additionally required, as will be shown below, were measured at each section in question by removing the interferometer from the light path. Since spectral lines of neutral argon have not been observed, the Doppler shifts were obtained from lines of singly ionized argon, especially from the line at 4348 Å.

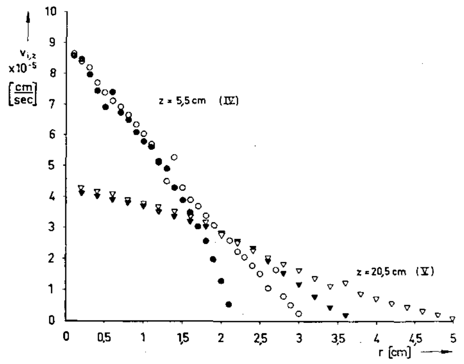

Fig. 4 Axial velocity profiles at Secs. IV and V.

Transformation

The transformation of the measured gross Doppler shift profiles to local quantities has been accomplished by using the intensity profiles and profiles of emission coefficients computed from these via an Abel transform as weights in a modified Abel transform for rotational and elliptical cases. Figure 3 shows profiles of integrated Doppler shifts, emission coefficients, and transformed local Doppler shifts; the utility of the transform is evident, especially if the profiles of the emission coefficient flatten in the region near the axis. If the geometry of the jet deviates considerably from cylinder symmetry, the accuracy of the results of the transform decreases with increasing radius.

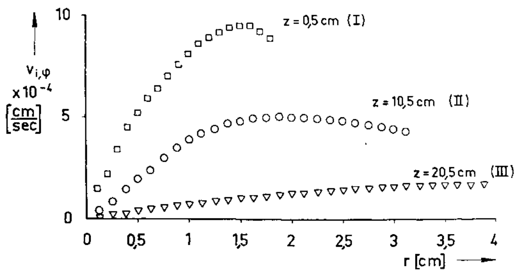

Fig. 5 Rotational velocity profiles at Secs. I, II, and III.

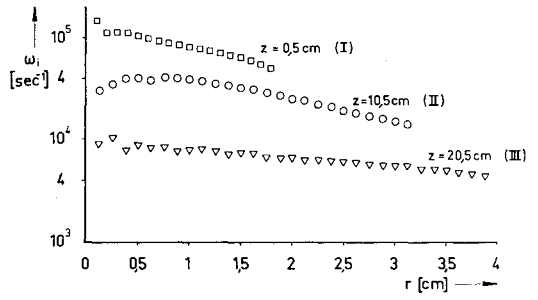

Fig. 6 Angular frequency of the jet vs radius at Secs. I, II, and III.

Results

Figures 4–6 show the profiles of axial and rotational velocity and the angular frequency, Fig. 6 illustrating the nonrigid-body rotation of the jet. A detailed description of experimental methods and transformation formulas may be found in previously published papers.[6,7]

References

[1] Kogelschatz, U., "Doppler Shift Measurements of Axial and Rational Velocities in an MPD Arc," AIAA Paper 69-110, New York, 1969; also *AIAA Journal*, to be published.

[2] Malliaris, A. C. and Libby, D. R., "Velocities of Neutral and Ionic Species in an MPD Flow," AIAA Paper 69-109, New York, 1969.

[3] Fradkin, D. B. et al., "Experiments Using a 25 kW Hollow Cathode Lithium Vapor MPD Arc Jet," AIAA Paper 69-241, Williamsburg, Va., 1969; also *AIAA Journal*, to be published.

[4] Connolly, D. J. and Sovie, R. J., "The Effect of Background Pressure and Magnetic Field Shape on MPD Thruster Performance," AIAA Paper 69-243, Williamsburg, Va., 1969.

[5] Krülle, G., "Characteristics and Local Analysis of MPD Thruster Operation," AIAA Paper 67-672, Colorado Springs, Colo., 1967.

[6] Beth, M.-U. et al., "Angular Velocity Profiles of a Rotating Argon Plasma Jet," Paper 6.2.4., VIIIth International Conference on Phenomena in Ionized Gases, Vienna, 1967.

[7] Bohn, W. L., Beth, M.-U., and Nedder, G., "On Spectroscopic Measurements of Velocity Profiles and Non-Equilibrium radial Temperatures in an Argon Plasma Jet," *Journal of Quantitative Spectroscopy and Radiative Transfer*, Vol. 7, 1967, pp. 661–676.

A Numerical Solution of the Conduction Problem with Radiating Surface

CAROLYN MASON*
McDonnell Douglas Astronautics Company, Santa Monica, Calif.

Nomenclature

Q = surface heat flux
c_p = specific heat
ρ = density
t = time
h = distance
K = thermal conductivity
α = thermal diffusivity
T = temperature
ϵ = emissivity

Received April 16, 1969; revision received July 15, 1969. This work was supported by the MDAC-WD Independent Research and Development Program.

* Computing Engineer, Information Processing System Department, Western Division.

σ = Stefan-Boltzman constant
h_c = heat transfer coefficient
I.S. = insulated surface
U.S. = uninsulated surface

Subscripts

i = space locations
m = convective medium
n = time sequence
w = wall
eq = equilibrium

Superscript

k = Runge-Kutta step

Introduction

TRADITIONALLY, the problem of transient heat conduction with a radiating surface has been solved in one of two ways: 1) an explicit Runge-Kutta integration, 2) a fully implicit difference method. The fully implicit method is unconditionally stable. However, radiation and convection are assumed to originate from the surface node, and an approximation to the radiation term is necessary to linearize the resulting difference equation.[1] The error due to this approximation can be kept to within 10% for temperatures greater than 5000°F.

A very accurate solution is possible with the explicit Runge-Kutta technique combined with an actual wall temperature computation, but the stability criterion associated with the explicit form of the difference equation may make this technique prohibitively expensive for fine meshes.[2]

Discussion

In the proposed method an implicit difference, which is unconditionally stable, is used between all interior points, and an explicit difference is used between the wall and adjacent node. In order to achieve reasonable accuracy in cases with a rapidly changing surface heat flux, a Runge-Kutta-type integration is imposed on the surface. A description follows.

The surface heat flux is computed by using Eqs. (1) and (2) with conditions at time t_n in Runge-Kutta step 1, at time $t_{n+1/2}$ in steps 2 and 3, and at time t_{n+1} in step 4;

$$-\epsilon\sigma T_w{}^4 + h_c(T_m - T_w) + [K/(\Delta h/2)](T_1 - T_w) = 0 \tag{1}$$

$$\dot{Q} = -\epsilon\sigma T_w{}^4 + h_c(T_m - T_w) \tag{2}$$

Interior temperatures are computed at time $t + \Delta t/2$ using Eqs. (3–5);

$$\left(1 + a\,\frac{\Delta t}{2}\right) T_1{}^{(k)} - a\,\frac{\Delta t}{2}\,T_2{}^{(k)} = T_{1,n} + \frac{Q^{(k)}}{\rho c \Delta h}\cdot\frac{\Delta t}{2} \tag{3}$$

$$-a\,\frac{\Delta t}{2}\,T_{i-1}{}^{(k)} + \left(1 + 2a\,\frac{\Delta t}{2}\right) T_i{}^{(k)} - a\,\frac{\Delta t}{2}\,T_{i+1}{}^{(k)} = T_{i,n} \tag{4}$$

$$-a(\Delta t/2)T_{N-1}{}^{(k)} + [1 + 2a(\Delta t/2)]T_N{}^{(k)} = T_{N,n} \tag{5}$$

where

$$a = \alpha/\Delta h^2$$

Table 1 Data for two cases

Data	Case I	Case II
Thickness	1.25 in.	0.09 in.
No. of laminae	25	15
C_P	0.1	0.4
K	0.1	0.17×10^{-4}
ρ	100	70
h_c	0.1	0.013323
T_m	10,000°F	3269°F
Initial temperature	100°F	100°F

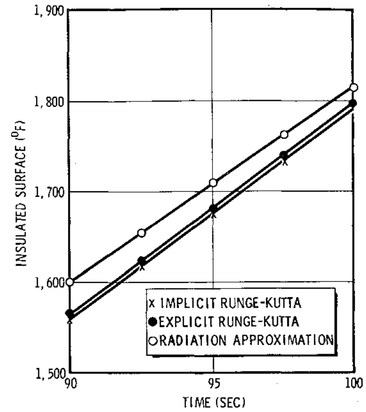

Fig. 1 Temperature history of insulated surface.

Final temperatures are obtained at time $t + \Delta t$:

$$T_{i,n+1} = T_{i,n} + \frac{\Delta t}{6}\left[\left(\frac{dT}{dt}\right)_i^{(1)} + 2\left(\frac{dT}{dt}\right)_i^{(2)} + 2\left(\frac{dT}{dt}\right)_i^{(3)} + \left(\frac{dT}{dt}\right)_i^{(4)}\right] \tag{6}$$

where

$$\left(\frac{dT}{dt}\right)_i^{(k)} = \frac{T_i{}^{(k)} - T_{i,n}}{\Delta t/2}$$

The stability criterion associated with the foregoing scheme is given by

$$\Delta t \leq \rho c \Delta h / Q(T_{eq} - T_1) \tag{7}$$

where

$$-\epsilon\sigma T_{eq}{}^4 + h_c(T_m - T_{eq}) = 0 \tag{8}$$

Examples

Data for the following two cases are given in Table 1 and results are given in Table 2.

Case I

In the first case considered, the external conditions were constant. As predicted for high surface temperatures, the radiation approximation differed from the explicit method by less than 1% at the surface. The implicit Runge-Kutta was slightly better. However, at the insulated surface the largest deviation recorded for the implicit Runge-Kutta was 0.25%; for the radiation approximation it was close to 2% (Fig. 1).

Case II

In the second case, a variable h_c and T_m were considered over a period of 325 sec. The maximum heating occurred at 10 sec, coincidentally with the largest deviations in surface temperature produced by the three methods. The radiation

Table 2 Results of three methods

Method	Explicit	Implicit	Implicit R-K
		Case I	
Δt	0.28	0.5	1.0
U.S.$_{max}$	5379.1510	5379.2132	5739.0405
Time	100	100	100
I.S.$_{max}$	1797.6192	1829.0741	1792.9188
Time	100	100	100
		Case II	
Δt	0.18	0.5	1.0
U.S.$_{max}$	1617.1977	1597.9562	1626.9853
Time	10	11	10
I.S.$_{max}$	641.8910	615.3460	642.9657
Time	250	250	250

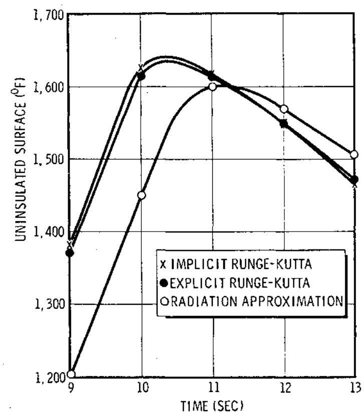

Fig. 2 Temperature history of uninsulated surface.

approximation showed an error of 7.5%. The implicit Runge-Kutta deviated by only 0.5% from the explicit method (Fig. 2).

Conclusion

The proposed method has been shown to be as accurate as the explicit Runge-Kutta. Unlike in the Runge-Kutta, the time increment is not dependent on the fineness of the mesh. In the example given, the implicit method was shown to execute four times faster than the explicit method with no significant difference in accuracy.

The implicit method combined with a Runge-Kutta integration on the surface conditions also has been shown to be significantly more accurate then the straight backward difference. In the example given there was no significant increase in execution time for the new method when using an equivalent compute interval.

The proposed method can be extended easily to composite materials and a variable mesh size. Also, the same method can be applied to the case with two exterior radiating surfaces. It should be possible to extend the method to two- and three-space dimensions by using a modification of the Douglas-Rachford method similar to that proposed by P.L.T. Brian.[3]

References

[1] Gaumer, G. R., "Stability of Three Finite Difference Methods of Solving Transient Temperatures," *ARS Journal*, Vol. 32, No. 10, Oct. 1962, pp. 1595–1597.

[2] Richtmeyer, R. D. and Morton, K. W., *Difference Methods for Initial Valve Problems*, 2nd ed., Interscience, New York, 1967, p. 189.

[3] Brian, P. L. T., "A Finite Difference Method of Higher-Order Accuracy for the Solution of Three-Dimensional Heat Conduction Problems," *A.I.Ch.E. Journal*, Vol. 7, No. 3, Sept. 1961, pp. 367–370.

Some Plane Quadrilateral "Hybrid" Finite Elements

Robert D. Cook* and Jaafar K. Al-Abdulla†
University of Wisconsin, Madison, Wis.

Introduction

In this Note the "hybrid" element of Pian[1] is generalized to arbitrary quadrilateral form. Four hybrids having constant and linear stress distributions are considered. An example problem is solved in order to compare the elements.

Received June 27, 1969. Thanks are expressed to the University Research Committee for providing computer time.

* Associate Professor, Department of Engineering Mechanics.
† Project Assistant, Mathematics Research Center.

Table 1 Matrix T for hybrids $H1$-$H4$

T	$H1$	$H2$	$H3$	$H4$	T	$H1$	$H2$	$H3$	$H4$
$T_{1,j}$	a	a	a	a	$T_{1,j+4}$	0	0	0	0
$T_{2,j}$	0	c	0	e	$T_{2,j+4}$	b	0	b	$-c$
$T_{3,j}$	b	0	b	c	$T_{3,j+4}$	a	b	a	0
$T_{4,j}$	...	0	e	0	$T_{4,j+4}$	...	d	$-c$	b
$T_{5,j}$	...	b	$-d$	0	$T_{5,j+4}$	...	a	$-e$	d
$T_{6,j}$	...	...	...	$-d$	$T_{6,j+4}$	...	...	...	$-e$
$T_{7,j}$	...	...	...	b	$T_{7,j+4}$	...	...	...	a

Hybrid elements considered are called $H1$, $H2$, $H3$, and $H4$. The notation of Pian[1] is used where possible. Thus $\boldsymbol{\sigma} = \mathbf{P}\boldsymbol{\beta}$, and the $\mathbf{P}$ matrices of the four hybrids are

$$H1 = \begin{bmatrix} 1 & 0 & 0 \\ 0 & 1 & 0 \\ 0 & 0 & 1 \end{bmatrix}, \quad H2 = \begin{bmatrix} 1 & y & 0 & 0 & 0 \\ 0 & 0 & 1 & x & 0 \\ 0 & 0 & 0 & 0 & 1 \end{bmatrix}$$

$$H3 = \begin{bmatrix} 1 & 0 & 0 & x & 0 \\ 0 & 1 & 0 & 0 & y \\ 0 & 0 & 1 & -y & -x \end{bmatrix}$$

$$H4 = \begin{bmatrix} 1 & x & y & 0 & 0 & 0 & 0 \\ 0 & 0 & 0 & 1 & x & y & 0 \\ 0 & -y & 0 & 0 & 0 & -x & 1 \end{bmatrix}$$

Formulation of Matrices

Consider an arbitrary quadrilateral of constant thickness t whose corners are numbered counterclockwise 1–4. Matrix $\mathbf{T}$ accounts for work done by boundary forces. Its form is determined by consideration of stress and displacement components in coordinate directions ns, where s coincides with the edge being treated, and the normal n makes a counterclockwise angle θ with respect to the x axis (plate elements have been similarly treated; see, e.g., Ref. 2). The analysis is as follows. First, express ns nodal displacements, four for each edge, in terms of nodal displacements in xy coordinates,

$$\underset{16\times 1}{\mathbf{q}'} = \underset{16\times 8}{\mathbf{W}} \; \underset{8\times 1}{\mathbf{q}}, \qquad W_{ij} = f_1(\theta) \tag{1}$$

Next, require that ns displacements along each edge be linear functions of s,

$$\underset{8\times 1}{\mathbf{u}'} = \underset{8\times 16}{\mathbf{L}'} \; \underset{16\times 1}{\mathbf{q}'}, \qquad L_{ij}' = f_2(s, l) \tag{2}$$

where l is the length of an edge. Next, express ns edge stresses in terms of $\boldsymbol{\beta}$,

$$\underset{8\times 1}{\mathbf{S}} = \underset{8\times 3}{\mathbf{Z}} \; \underset{3\times 1}{\boldsymbol{\sigma}} = \mathbf{Z}\mathbf{P}\boldsymbol{\beta}, \qquad Z_{ij} = f_3(\theta) \tag{3}$$

In $\mathbf{P}$, for example, along edge 1-2 we have $x = x_1 - s\sin\theta_{12} = x_1 - s(x_1 - x_2)/l_{12}$. Finally, matrix $\mathbf{T}$ results from integration of $(\mathbf{ZP})^T\mathbf{L}'\mathbf{W} = \mathbf{R}^T\mathbf{L}$ along the edges. Let

$$\begin{aligned} a &= t(y_k - y_i)/2, \; b = t(x_i - x_k)/2 \\ c &= t[y_k(y_j + y_k) - y_i(y_i + y_j)]/6 \\ d &= t[x_i(x_i + x_j) - x_k(x_j + x_k)]/6 \\ e &= t[y_j(x_k - x_i) + x_j(y_k - y_i) + 2(x_k y_k - x_i y_i)]/6 \end{aligned} \tag{4}$$

where i, j, k are cyclically permuted from 1–4 and $i = j - 1$,

Table 2 Times in milliseconds on CDC 3600 computer to form stiffness matrix and to compute and print stresses. Trace of stiffness matrix for square element with modulus $E = 1.0$ and Poisson's ratio $\nu = \frac{1}{3}$

Property	$H1$	$H2$	$H3$	$H4$	$I1$	$I4$	$T4$
Formation	17	60	60	92	16	50	110
Stresses	28[a]	185	185	214	142	142	...
Trace	3.00	3.67	3.18	3.75	3.00	4.00	4.13

[a] Stresses at one point only.